Harnessing Fluid-Driven Vesicles To Pick Up and Drop Off Janus Particles

Isaac Salib,[†] Xin Yong,[†] Emily J. Crabb,[‡] Nicholas M. Moellers,[‡] Gerald T. McFarlin IV, Olga Kuksenok, and Anna C. Balazs*

Chemical Engineering Department, University of Pittsburgh, Pittsburgh, Pennsylvania 15261, United States. [†]These authors contributed equally to this work. [‡]These undergraduate authors contributed equally to this work.

ABSTRACT Using dissipative particle dynamics (DPD) simulations, we model the interaction between nanoscopic lipid vesicles and Janus nanoparticles in the presence of an imposed flow. Both the vesicle and Janus nanoparticles are localized on a hydrophilic substrate and immersed in a hydrophilic solution. The fluid-driven vesicle successfully picks up Janus particles on the substrate and transports these particles as cargo along the surface. The vesicle can carry up to four particles as its payload. Hence, the vesicles can act as nanoscopic "vacuum cleaners", collecting nanoscopic debris localized on the floors of the fluidic devices. Importantly, these studies reveal how an imposed flow can facilitate the incorporation of nanoparticles into nanoscale vesicles. With the introduction of a "sticky" domain on the substrate, the vesicles can also robustly drop off and deposit the particles on the surface. The controlled pickup and delivery of nanoparticles *via* lipid vesicles can play an important step in the bottom-up assembly of these nanoparticles within small-scale fluidic devices.

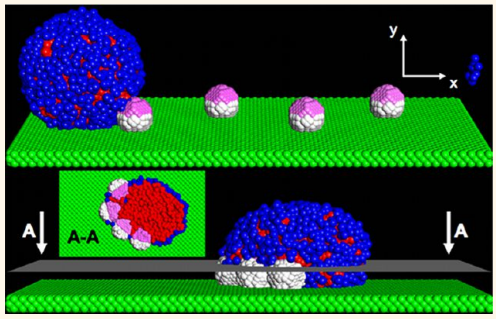

KEYWORDS: fluid-driven vesicles · Janus particles · dissipative particle dynamics · endocytosis · microfluidics · lipid membrane

Micro- and nanofluidic devices provide useful environments for achieving distinct forms of self-assembly since the imposed flow within the fluid-filled chamber can potentially guide the self-organization processes. On the other hand, bottom-up forms of self-assembly within these devices would be greatly aided by establishing effective means of picking up a specific component and controllably moving that component to a particular location on the floor of the fluidic chamber. In effect, the ideal carrier for these applications might be synthetic analogues of osteoclast and osteoblast cells. In the most general sense, the osteoclasts pick up particulates from the surface of bone and osteoblasts controllably deposit material on this surface. It is this controlled adsorption and deposition of particles onto a surface that would be desirable to mimic *via* synthetic nano- or microcarriers within fluidic devices.

In designing such biomimetic cargo carriers, it is useful to recall that lipid vesicles offer unique opportunities for encapsulating a range of species, including nanoparticles, within their cores and transporting these payloads to targeted locations in fluidic environments. For example, nanoscopic lipid vesicles can serve as nanocontainers that transport cargo into biological cells, making these ideal systems for drug delivery.[1] To optimize the performance of lipid vesicles in these and other applications, researchers have utilized computational modeling to isolate factors that enable the vesicles to encapsulate various types of nanoparticles. These studies have revealed how not only the shape[2−4] but also the chemical composition[5,6] (*i.e.*, relative fraction of hydrophobic and hydrophilic sites on the particle's surface) affect the penetration of the nanoparticles into the vesicles. Notably, most of these computational studies[2,4−6] have considered scenarios where the size of the vesicles is relatively large compared to the size of the nanoparticles, and hence, the simulations have focused on the interactions of the nanoparticles with a single, relatively flat lipid bilayer. With the rapidly growing ability to control the size and polydispersity of nanoscale lipid vesicles[1] and the expanded utility of these assemblies as nanoreactors,[7] it becomes useful to focus on such small-scale vesicles and probe their interactions with potential payloads.

* Address correspondence to balazs@pitt.edu.

Received for review October 5, 2012 and accepted January 30, 2013.

Published online January 30, 2013
10.1021/nn304622f

Herein, we use computational modeling to investigate the interactions of a nanoscale lipid vesicle and spherical Janus nanoparticles, which contain both hydrophilic and hydrophobic regions. Through these studies, we devise an approach that exploits the flow fields in a channel and utilizes fluid-driven lipid vesicles to effectively pick up nanoparticles located on a substrate and controllably move these particles along the surface. We also establish means of driving these carriers to drop off their cargo at particular sites in the channel.

In these simulations, we specifically focus on vesicles localized on a hydrophilic substrate and immersed in a hydrophilic solution. We introduce an imposed shear flow to drive the vesicles toward the nanoparticles and determine conditions that enable the vesicle to pick up this cargo and transport it along the surface. To the best of our knowledge, these are the first computational studies to consider the role of an imposed flow on the vesicle–nanoparticle interactions. Understanding the effect of the imposed flow is vital for designing effective cargo carriers in microfluidic devices. Furthermore, studies on the behavior of vesicle–particle assemblies in a flow field are also important for gaining insight into the performance of nanocarriers in the bloodstream.

As we show below, the vesicles can act as nanoscopic "vacuum cleaners", collecting and absorbing the Janus particles that they encounter along their paths. This distinct ability depends on the shear rate, the composition of the nanoparticles, and the adhesion strength between the nanoparticles and the substrate. We demonstrate that there is a range of shear rates for which the vesicle can even adsorb Janus particles encompassing just a small fraction of hydrophobic sites. Furthermore, a single vesicle can take up and transport a number of these particulates. Notably, the vesicles remain intact and retain the nanoparticles as the entire assembly is driven to move along the substrate. It is noteworthy that the action of these lipid vesicles roughly resembles the behavior of the osteoclasts. Used in a microfluidic device, these vesicles can be harnessed to remove nanoscopic "dirt" or debris from hydrophilic substrates that need to be relatively clean for their functionality (*e.g.*, cell growth studies). More generally, these studies reveal how an imposed flow can facilitate the incorporation of nanoparticles into nanoscale vesicles.

We also show how the introduction of an adhesive patch on the substrate can be utilized to achieve the effective drop off of the adsorbed nanoparticles. In this sense, the vesicles also mimic osteoblasts since they deliver species to particular locations on a substrate. Overall, our findings can provide new routes for manipulating the assembly of nanoscopic particles in solution.

In carrying out these studies, we utilize the dissipative particles dynamics (DPD) method[8−12] to model the interactions among the vesicles, nanoscopic Janus particles, and solvent. The DPD is a mesoscopic approach that is similar to coarse-grained molecular dynamics (MD) simulations and allows one to capture the hydrodynamics of complex fluids while retaining essential information about the structural properties of the system's components. Unlike MD simulations, however, DPD utilizes soft repulsive interactions between the beads, which represent clusters of molecules. Consequently, one can use a significantly larger time step, Δt, between successive iterations than those required by MD simulations. This, in turn, allows the DPD approach to be used to model physical phenomena occurring at time and spatial scales many orders of magnitude greater than that captured by MD. Notably, the DPD also differs from MD by using a momentum-conserving thermostat.[10,12] We mention that the DPD method has some limitations with respect to accurately modeling fluid–solid boundaries and liquid–vapor coexistence,[13,14] but these limitations are not critical to obtaining the results presented here. In the Methodology section, we describe the DPD technique in greater detail; we then discuss our findings on the interactions between nanoscopic vesicles (Figure 1a), which are self-assembled from twin-tailed lipids (Figure 1b), and Janus particles (Figure 1c) moving on a substrate in the presence of an applied flow.

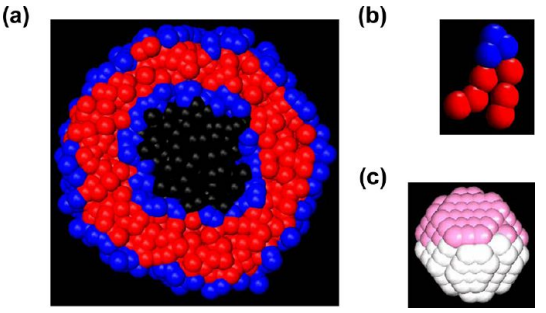

Figure 1. (a) Vesicle self-assembled from 586 twin-tailed lipids dispersed in a hydrophilic solvent (not displayed); black beads are inner solution. (b) Schematic of a coarse-grained model of a twin-tailed lipid; blue beads are hydrophilic head, and red beads are hydrophobic tails. (c) Schematic of a Janus particle, formed from 392 DPD beads of which 196 beads are hydrophilic (white) and 196 beads are hydrophobic (pink). The beads are arranged in a face-centered cubic lattice structure with a cube side of 0.7.

RESULTS AND DISCUSSION

Interaction between a Lipid Vesicle and a Single Particle. *Symmetric Janus Particle and Pure Hydrophilic Particle.* We first focus on determining the conditions under which a nanoscale lipid vesicle can "pick up" and transport nanoparticles. As our reference case, we consider the interaction between a lipid vesicle and a single symmetric Janus particle (the fraction of hydrophobic beads being $\phi = 0.5$), where the substrate–lipid and substrate–particle bonding interactions are characterized by the respective bond constants of

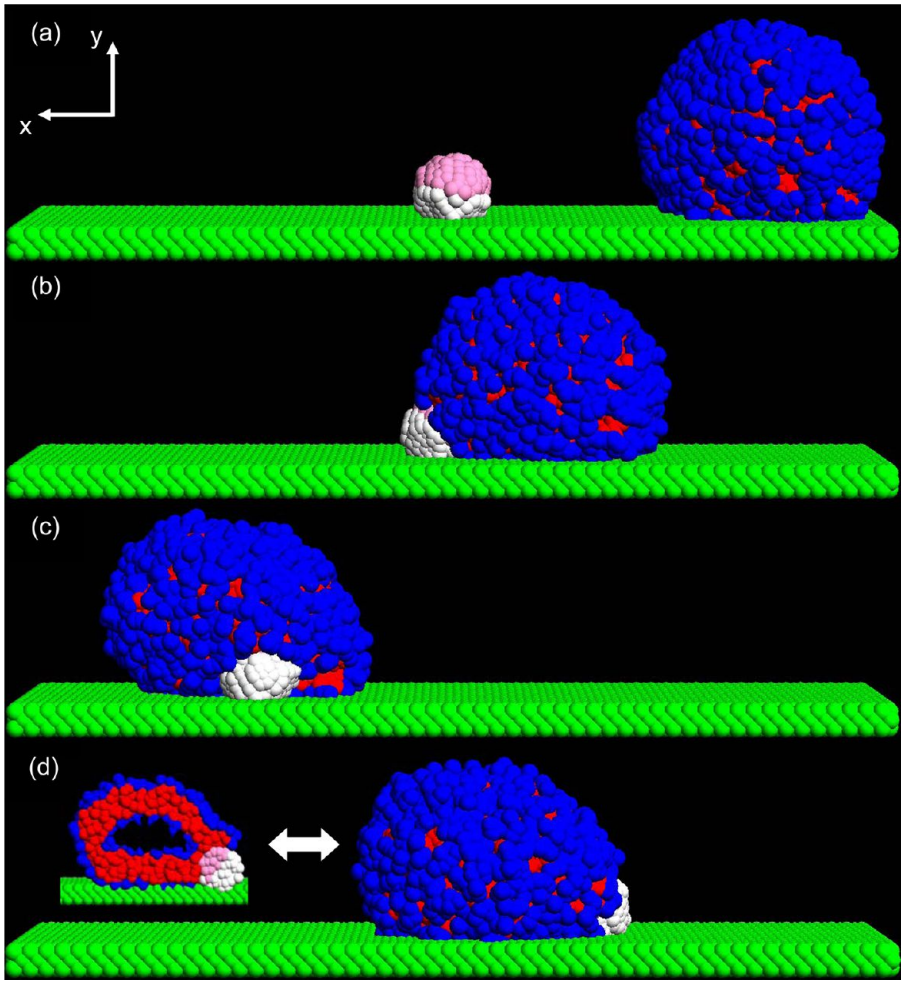

Figure 2. Snapshots of the system with a symmetric Janus particle (*i.e.*, with fraction of hydrophobic beads $\phi = 0.500$) for shear rate $\dot{\gamma} = 0.015$. The substrate beads are colored green. Here, we set $K_{sub/lipid} = 4$ and $K_{sub/Janus} = 8$ and the shear flow is in positive *x*-direction (from right to left). The snapshots are taken for times (a) 50, (b) 330, (c) 680, and (d) 3940. The inset in (d) is the cross-sectional view of the vesicle and the attached Janus particle, which shows that the hydrophobic part of the Janus particle is absorbed into the hydrophobic part of the vesicle membrane.

$K_{sub/lipid} = 4$ and $K_{sub/Janus} = 8$ and the shear rate for the fluid is $\dot{\gamma} = 0.015$.

Initially, we place the Janus particle on the substrate relatively far from the lipid vesicle. (The initial distance between the centers of a particle and a vesicle is set at 22.5.) Hence, at early times, the vesicle has not yet made contact with the Janus particle and the hydrophobic portion of the particle is exposed to the hydrophilic solution (see Figure 2a). The shear flow drives the vesicle along the substrate (from right to left in Figure 2), and when the vesicle makes contact with the particle, the hydrophobic half of the particle penetrates into the bilayer lipid membrane (Figure 2b). The hydrophobic−hydrophobic interactions between the hydrophobic particle beads and the lipid tails are more energetically favorable than the hydrophobic−hydrophilic interactions between the particle beads and the outer solution. Because of this energetically favorable interaction, the hydrophobic portion of the particle remains immersed in the hydrophobic part of the vesicle membrane for the remainder of the simulation, and the particle is dragged along by the vesicle as the entire assembly is driven by the shear flow to the left (Figure 2c,d). The absorption of the hydrophobic part of the Janus particle into the hydrophobic part of the vesicle membrane can be seen more clearly in the inset in Figure 2d, which is a cross-sectional view of the particle and vesicle at the moment in the simulation depicted in Figure 2d.

To quantify the process of the vesicle membrane absorbing the hydrophobic portion of the Janus particle seen in Figure 2, we calculate the number of hydrophobic Janus particle bead/lipid tail interactions and the number of hydrophobic Janus particle bead/outer solution bead interactions; these two data sets are plotted *versus* time in Figure 3. The number of interactions is defined as the number of pairs of hydrophobic particle beads and lipid tail beads or hydrophobic particle beads and outer solution beads that are separated by a distance smaller than r_c.[15] By monitoring these two types of interactions, we can determine quantitatively when the vesicle picks up the

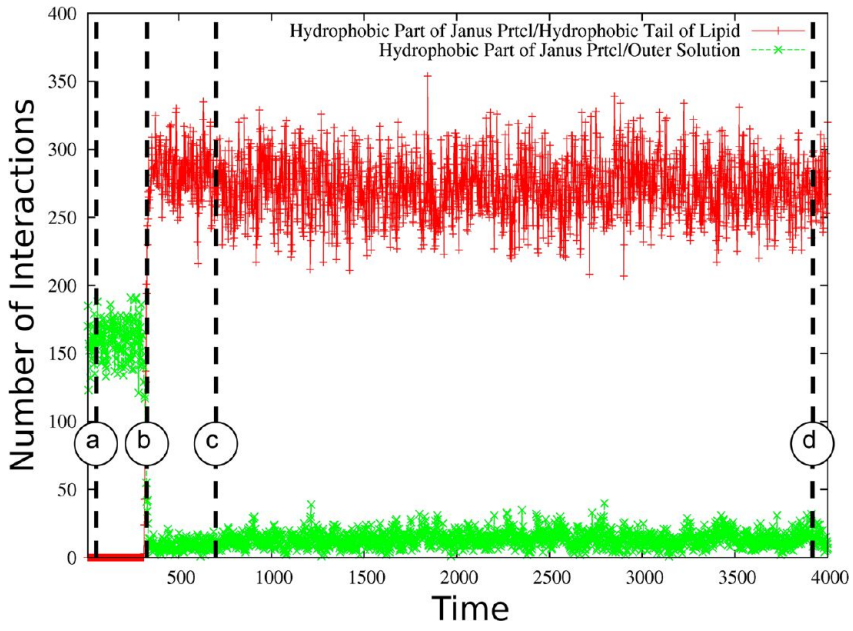

Figure 3. Temporal evolution of the number of interactions between the hydrophobic beads of the Janus particle and the outer solution beads (green crosses) and between the hydrophobic beads of the Janus particle and the hydrophobic lipid tail beads (red pluses), for the simulation shown in Figure 2. The annotations with the letters a–d correspond to the frames Figure 2a–d, respectively.

particle and how much of the hydrophobic portion of the particle is immersed in the vesicle. As the Janus particle in our simulation encounters the vesicle at $t \sim 320$ (labeled as b on Figure 3), the hydrophobic part of the particle gets absorbed almost instantaneously into the hydrophobic interior of the vesicle membrane, and thus, the vesicle membrane shields the hydrophobic beads of the Janus particle from interacting with the outer hydrophilic solution. This adsorption occurs essentially instantaneously; that is, it takes only approximately ~25 dimensionless units of time, which corresponds to ~0.18 μs according to the scaling provided in the Methodology section. This rapid absorption is represented by the sharp increase in the number of hydrophobic particle bead/lipid tail interactions and the associated drastic decrease in the number of hydrophobic particle bead/outer solution interactions.

Figure 3 also shows that the number of each type of interaction fluctuates around a constant value after the particle is adsorbed by the vesicle. Therefore, most of the hydrophobic half of the Janus particle remains shielded from the outer hydrophilic solution by the vesicle's lipid membrane, as was seen in the inset of Figure 2d. In other words, after the Janus particle–vesicle assembly is formed, it remains stable and can be successfully transported by the imposed shear flow. This absorption of the symmetric Janus particle by the vesicle is robust and is observed for a range of shear rates and interactions between the particle and the substrate, as we show below.

In order to determine the effect of the chemical composition of the nanoparticle on its ability to penetrate the vesicle, we ran simulations using a particle composed solely of hydrophilic beads. As anticipated from the above discussion, our simulations show that the vesicle does not pick up a purely hydrophilic particle. Rather, as shown in Figure 4, the vesicle pushes the hydrophilic particle out of its path as it moves along the surface. The particle is not absorbed into the bilayer lipid membrane because it is more energetically favorable for these hydrophilic beads to remain in contact with the hydrophilic solvent and hydrophilic substrate than to be in contact with the hydrophobic lipid tails.

To gain further insight into the factors that control the motion of the Janus particle–vesicle assembly (such as that in Figure 2d), we measure the speed of the attached Janus particle at different shear rates and adhesion strengths. Figure 5a shows the displacement *versus* time for one simulation run for a symmetric Janus particle and a bond constant of $K_{sub/Janus} = 8$ at each of the following three shear rates: $\dot{\gamma} = 0.015, 0.025,$ and 0.035. Initially, the particle displacement is equal to 0; however, after this particle is picked up by the vesicle, its displacement increases at an approximately constant rate. The speed of the particle is then obtained by calculating the slope of displacement *versus* time. The speeds of the Janus particles for simulation runs using $6 \leq K_{sub/Janus} \leq 12$ and $0.015 \leq \dot{\gamma} \leq 0.035$ are displayed in Figure 5b. The figure shows that the speed of the particle's motion increases at higher shear rates and decreases at greater adhesion strengths between the hydrophilic particle beads and the substrate. In other words, increasing the imposed flow propels the vesicle and its attached particle faster, while the

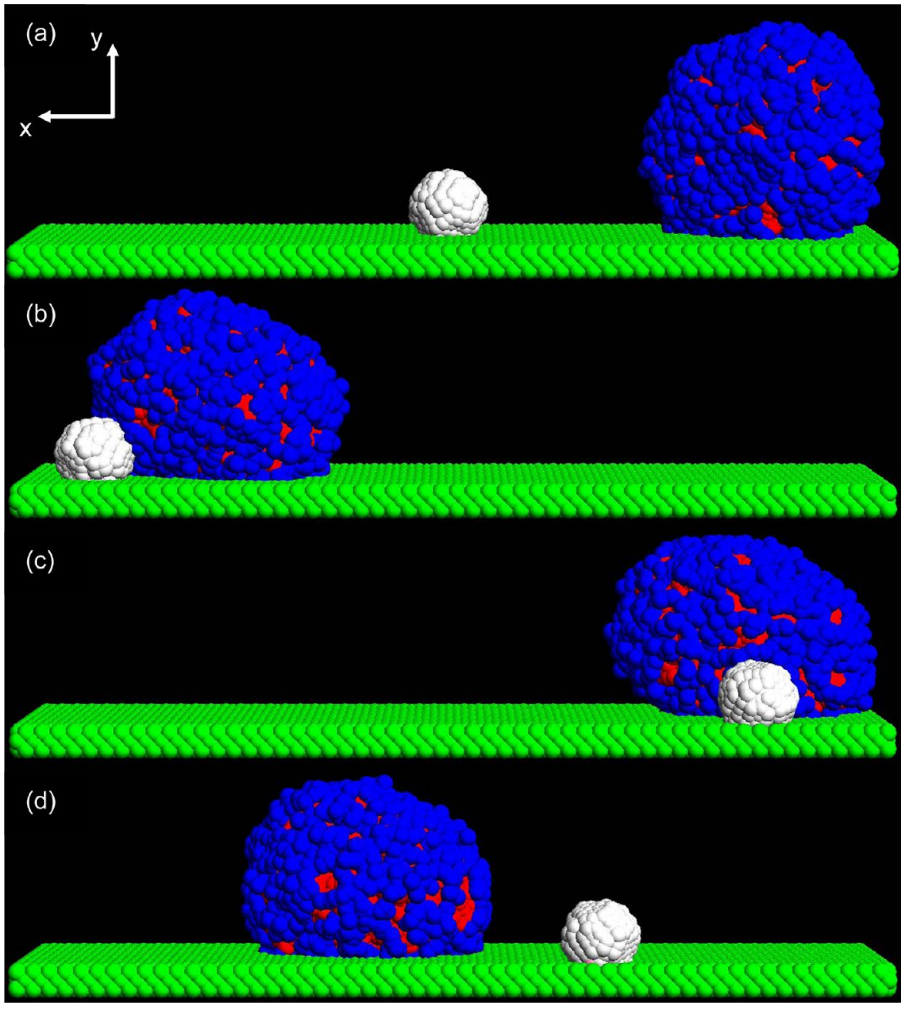

Figure 4. Snapshots of the system with purely hydrophilic particle for shear rate $\dot{\gamma} = 0.015$, $K_{sub/lipid} = 4$, and $K_{sub/Janus} = 8$. The snapshots are taken for times (a) 2, (b) 698, (c) 1038, and (d) 1502.

adhesion between the particle and the substrate induces a friction force that opposes the motion caused by the shear and, hence, slows down the motion of the assembly. Note that the speed also corresponds to the fact that the dynamics of the Janus particle−vesicle assembly is dominated by advection.

Asymmetric Janus Particles. As shown above, the symmetric Janus particle was adsorbed and transported by the moving vesicle, but the purely hydrophilic particle remained unattached. To determine the fraction of hydrophobic beads within the Janus particle, ϕ, that are necessary for the particle to be picked up by the fluid-driven vesicle, we systematically varied ϕ in the range $0 < \phi < 0.5$. The lowest fraction considered here, $\phi = 0.010$, corresponds to a total of four hydrophobic beads.

We find that for a shear rate of $\dot{\gamma} = 0.015$ and bond constants of $K_{sub/lipid} = 4$ and $K_{sub/Janus} = 8$, all of the nonzero fractions of hydrophobic beads considered here (within the range $0 < \phi < 0.5$) result in the particle being adsorbed and carried by the vesicle. We performed four independent runs per each value of ϕ. Figure S1 (Supporting Information) displays the graphic output from the simulations for the case of $\phi = 0.010$. Following the same procedure as described above, this particle is initially placed far from the vesicle. As the vesicle comes in contact with the particle, the hydrophobic beads on this highly asymmetric Janus sphere penetrate into the hydrophobic interior of the lipid membrane, where they are shielded from the external hydrophilic solvent, as can be seen in the inset of Figure S1d. After the particle becomes adsorbed, it is dragged behind the vesicle for the remainder of the simulation, with its hydrophobic beads remaining in the more energetically favorable position inside the lipid bilayer.

To enhance our understanding of this pick up process, we vary the shear rate and the particle−substrate adhesion strength in the respective ranges of $0.015 \leq \dot{\gamma} \leq 0.035$ and $6 \leq K_{sub/Janus} \leq 12$. With these simulations, we generate the phase map shown in Figure S2, which indicates the results of all four independent simulations for each data point. At the lowest shear rate, $\dot{\gamma} = 0.015$, the particle is picked up

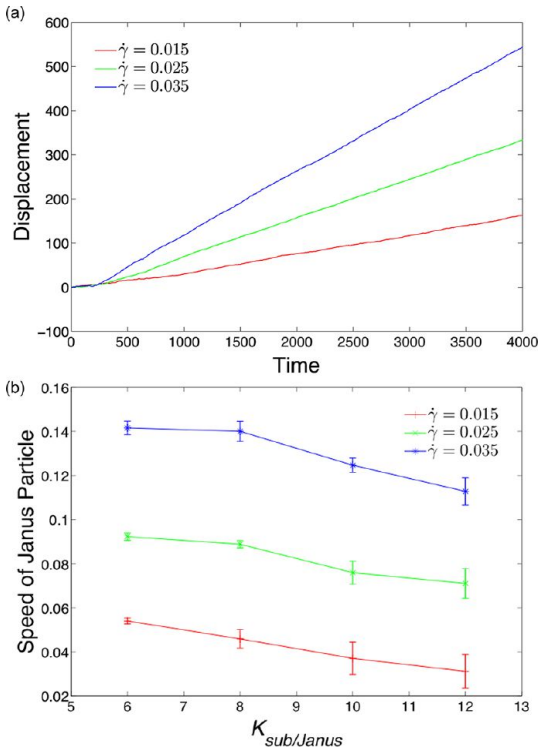

Figure 5. (a) Displacement of the attached Janus particle (ϕ = 0.500) along the *x*-axis for simulations conducted for three shear rates, $\dot{\gamma}$ = 0.015, 0.025, and 0.035, and bond constants $K_{sub/lipid}$ = 4 and $K_{sub/Janus}$ = 8. Each curve corresponds to a single simulation run. (b) Speed of the attached Janus particle along the *x*-axis as a function of $K_{sub/Janus}$ for three shear rates, $\dot{\gamma}$ = 0.015, 0.025, and 0.035. Each point is an average of four independent runs.

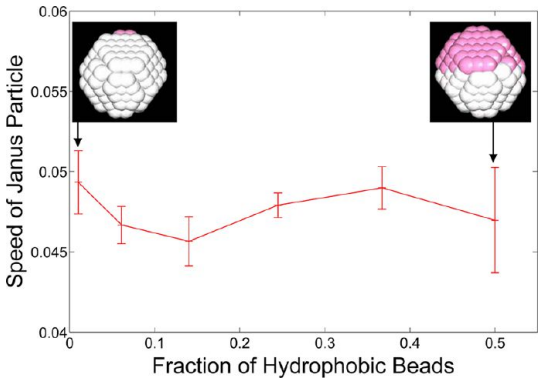

Figure 6. Speed of the attached Janus particle, with different ratios of hydrophobic beads ϕ = 0.500, 0.367, 0.245, 0.140, 0.061, and 0.010, along the *x*-axis for shear rate $\dot{\gamma}$ = 0.015, $K_{sub/lipid}$ = 4, and $K_{sub/Janus}$ = 8. Each point is an average of four independent runs.

and transported by the vesicle quite robustly for each $K_{sub/Janus}$ and $0 < \phi < 0.5$ examined. The notable exceptions occur for some runs involving the ϕ = 0.010 particle at $K_{sub/Janus}$ = 10 and 12; in these cases, the predominately hydrophilic particle either is not picked up (one run at $K_{sub/Janus}$ = 10) or is picked up and later dropped by the vesicle (one run with $K_{sub/Janus}$ =12). In other words, as can be seen from Figure S2a, the low shear rate facilitates the transport of particles by the moving vesicle.

As the shear rate is increased to $\dot{\gamma}$ = 0.025, the particles are picked up for $K_{sub/Janus}$ = 8 at all nonzero ϕ considered here, and the vesicle–Janus particle assembly is transported robustly along the substrate. When the adhesion strength between the substrate and particle is increased to $K_{sub/Janus}$ = 10, the fate of the ϕ = 0.010 particle is significantly affected. In three of the cases, it is picked up but ultimately becomes detached from the nanocarrier and is not even picked up in one of the simulations. All other Janus particles are picked up and carried along by the moving vesicle. When $K_{sub/Janus}$ is increased to 12, the vesicle can only pick up the particles robustly when they encompass a fraction $\phi \geq 0.365$. Notably, this phase map shows the appearance of catastrophic events that can occur in the system. Namely, the vesicles can be ruptured, and as a result, either the internal fluid gradually leaks out through the vesicle's membrane or the adsorbed particles tear off lipids from the membrane as they become detached from the vesicle. A comparison of Figure S2a,b highlights the damaging effects of increasing the shear rate.

With further increases in $\dot{\gamma}$, catastrophic events become more prevalent. At $\dot{\gamma}$ = 0.035, Figure S2c reveals instances at $K_{sub/Janus}$ = 8 where the vesicle not only drops its cargo but also undergoes catastrophic breakage. For $K_{sub/Janus}$ = 10 and 12, successful pick up events occur only sporadically, and there is a significant probability that the vesicles are destroyed in the process of carrying its cargo.

Summarizing the data in the phase map, we find that a particle with a greater fraction of hydrophobic beads (*i.e.*, larger ϕ) has a higher probability to be picked up by the vesicle because the favorable enthalpic interactions scale with the size of the hydrophobic portion. The value of $K_{sub/Janus}$ determines the "stickiness" of the substrate, and higher values of $K_{sub/Janus}$ lead to greater friction between the vesicle–particle and the surface and, thus, inhibit successful pickup. Similarly, higher shear rates are also detrimental to the pick up process. Here, the greater difference in the relative velocities between the mobile vesicle and the particle when these two species make contact can lead to their subsequent separation, even if the hydrophobic portion of the particles becomes immersed in the lipid membrane.

Finally, we compare the average speeds of picked up particles that encompass different fractions of hydrophobic beads; here, the shear rate is fixed at $\dot{\gamma}$ = 0.015 and bond strengths are set to $K_{sub/lipid}$ = 4 and $K_{sub/Janus}$ = 8. As can be seen in Figure 6, the error bars associated with the different particles' speeds overlap, so there is no statistically significant correlation between fractions of hydrophobic beads and the particle's speed. The fraction of hydrophobic beads may not greatly affect the particle's speed because the number

of interactions between the hydrophilic particle beads and the substrate and the number of interactions between the hydrophilic lipid heads of the vesicle and the substrate do not depend significantly on ϕ. As the hydrophilic−hydrophilic interactions with the substrate are the source of the friction force opposing the motion caused by the shear flow and the number of these interactions is similar for hydrophobic ratios $0 < \phi < 0.5$, the speed of the particle is not greatly influenced by its fraction of hydrophobic beads.

Interaction between Multiple Particles and a Lipid Vesicle. To achieve bottom-up assembly of the nanoparticles within a micro- or nanofluidic device, it would be useful for the vesicles to controllably transport more than just one particle to a particular location. To determine the ability of a vesicle to pick up and carry a larger payload, we placed a number of Janus particles characterized by $\phi = 0.37$ at equal distances from each other on the substrate. (Namely, the initial *x*- and *z*-coordinates of the N_p Janus particles on the substrate are separated by the distances $3L_x/4N_p$ and $L_z/4$, respectively, where L_x and L_z are the box sizes in the *x*- and *z*-directions.) For the multiple particle simulations, the width of the simulation box is extended to accommodate the additional Janus particles and prevent the deformed vesicle from forming a continuous vesicular bilayer structure in the periodic *z*-direction. The dimensions of the simulation box in the respective *x*-, *y*-, and z-directions are now $60.5 \times 40.0 \times 29.7$, with periodic boundary conditions being applied in the *x*- and *z*-directions.

We stipulate that, for a successful pickup, the vesicle must accomplish all of the following: (1) "grab" the particles, (2) transport the particles along the surface, (3) not leak its inner solution, and (4) not rupture. If any of these four requirements are not met, then the event is considered an unsuccessful pickup. When all four independent simulations for a given number of particles on the substrate exhibit successful pickups, we consider the behavior to be robust. After 22 000, the only scenario that displayed such robust behavior was the case involving four particles, as shown in Figure 7. The case involving six particles yielded one unsuccessful pickup out of four runs, and all runs displayed unsuccessful pickups for eight particles. It can be anticipated that simulations involving an even greater number of particles would also prove to be unsuccessful in meeting all four of the criteria noted above.

While the deformation of a vesicle is visible even in the case of just one adsorbed Janus particle, it is particularly pronounced in the cases involving multiple adsorbed particles. To characterize this spatial deformation, we calculate the relative shape anisotropy, κ^2, which is given by $\kappa^2 = [(\lambda_x - \lambda_y)^2 + (\lambda_y - \lambda_z)^2 + (\lambda_z - \lambda_x)^2]/2R_g^4$, where λ_x, λ_y, and λ_z are the eigenvalues of the gyration tensor **S** with $S_{mn} = 1/N\sum_{i=1}^{N} r_m^i r_n^i$. Here, *N* is the total number of lipid beads (hydrophobic and hydrophilic) and $\mathbf{r}^i$ is the position vector of the center of the *i*th bead with respect to the center of mass of the vesicle. The radius of gyration, R_g, is calculated as $R_g^2 = \lambda_x + \lambda_y + \lambda_z$.[16] The relative shape anisotropy for an ideal sphere is 0, and that for an ideal rod is 1. We note that the radius of gyration of the self-assembled vesicle[17] (Figure 1a) prior to its interaction with the substrate calculated using the above approach yields $R_g = 6.03$. This value is in a good agreement with the theoretical expression for the spherical shell, $R_g^2 = [3(R_o^5 - R_i^5)]/[5(R_o^3 - R_i^3)]$, where $R_o = 7.50$ and $R_i = 3.91$ are the outer and inner radii of the vesicle, respectively.[17]

To quantify the process of picking up of multiple particles for the scenario shown in Figure 7, we calculate the time evolution of the relative shape anisotropy and the total number of relevant interactions (Figure 8). Much as we did for the case of a single particle, we calculate the number of interactions between hydrophobic lipid tail beads and hydrophobic Janus particle beads, as well as the number of interactions between hydrophobic Janus particle beads and outer solution beads. Here, the total number of interactions involves a summation of the interactions on each Janus particle. With these measurements, we can determine the time at which a particle is absorbed by the mobile vesicle.

The relative shape anisotropy of the vesicle, κ^2, is plotted as a function of time in the upper graph in Figure 8; the number of interactions is plotted for the same time scale in the lower graph. The label annotations in Figure 8 correspond to the snapshots in Figure 7. The vesicle responds to each new particle that it picks up with a corresponding change in κ^2. After all four particles are picked up, the structure of the whole assembly remains the same until the end of the simulation, at 22 000. We compare the late-time value of κ^2 for a vesicle with four particles to the corresponding value for a vesicle with zero particles, calculated using an average of the last 100 frames for all four runs. Note that values of κ^2 remain relatively constant for these late times. The average final value of κ^2 for the case with four particles is 0.2773 ± 0.0225, as compared to 0.2201 ± 0.0193 in the case with zero particles. (Note that the relatively high value of κ^2 for a vesicle without the particles is a result of its attraction to the substrate; on the other hand, the same vesicle in the solution (as in Figure 1a) retains a nearly spherical shape with $\kappa^2 \approx 0.074$.)

It is noteworthy that, in the cases involving multiple Janus particles, these particles tend to aggregate into a large cluster on the substrate before they are adsorbed by the vesicle. By forming these clusters, some of the hydrophobic beads from multiple particles come in contact and thus can be shielded from hydrophilic components in solution and on the substrate. This particle aggregation can be seen in Figure S3 from both the inset snapshot and from the large number of

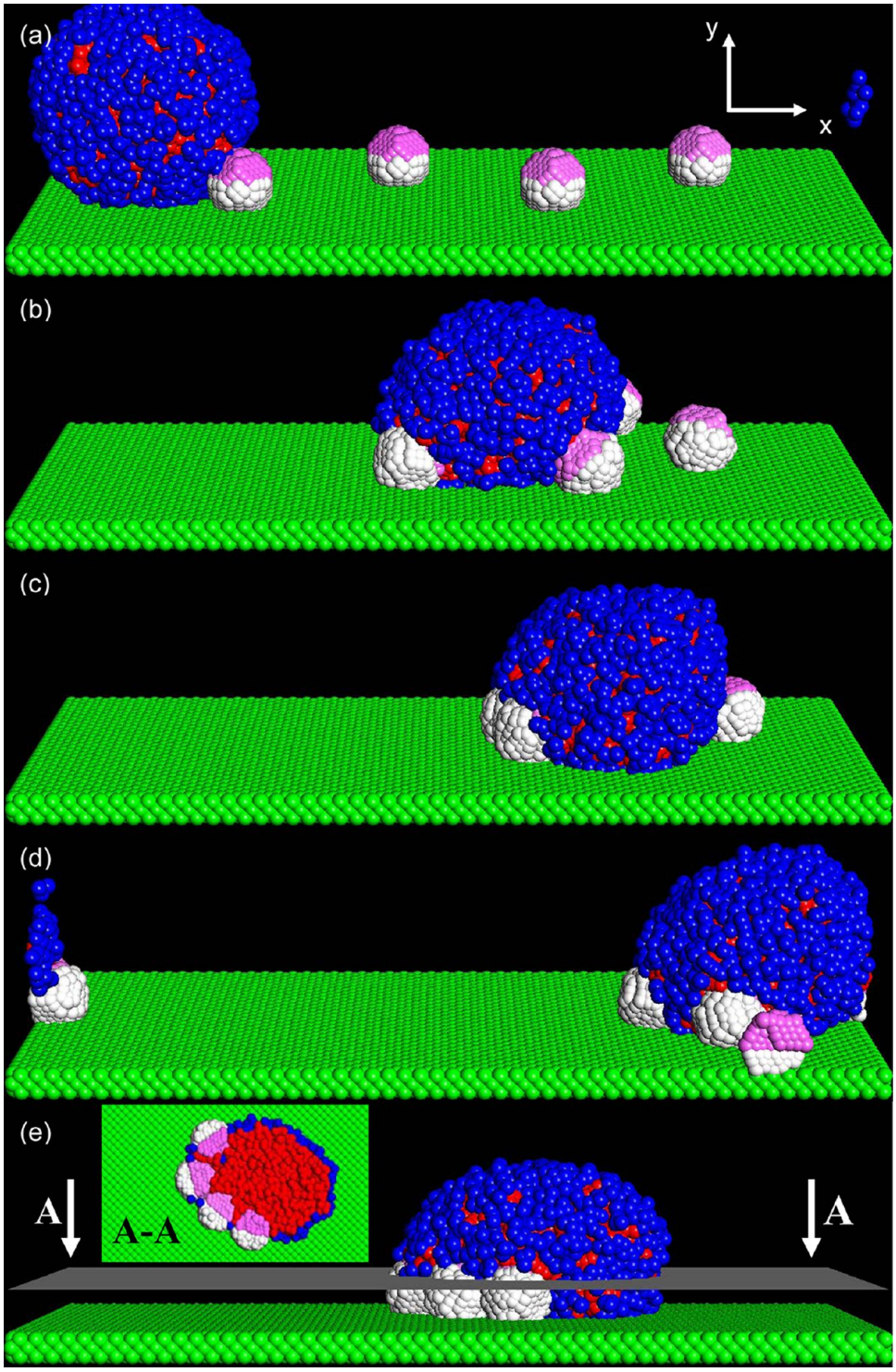

Figure 7. Snapshots of the system with four Janus particles with ϕ = 0.367. The snapshots are taken for times (a) 0, (b) 558, (c) 894, (d) 3444, and (e) 9960. The inset in (e) is the cross-sectional view of the vesicle−Janus particle assembly for the cutting plane A−A.

hydrophobic interparticle interactions. Notably, it is more difficult for the vesicle to pick up an entire cluster than it is to pick up a single particle. When the vesicle picks up each particle sequentially, the time separation between each pickup allows the vesicle to relax the strain induced by absorbing the particle, and the vesicle remains intact. However, when the vesicle attempts to absorb a cluster of particles simultaneously, the sudden distortion is significant. The large instantaneous stress on the lipid membrane could easily cause either leakage or rupture of the vesicle, and it is more probable that the pickup will be unsuccessful.

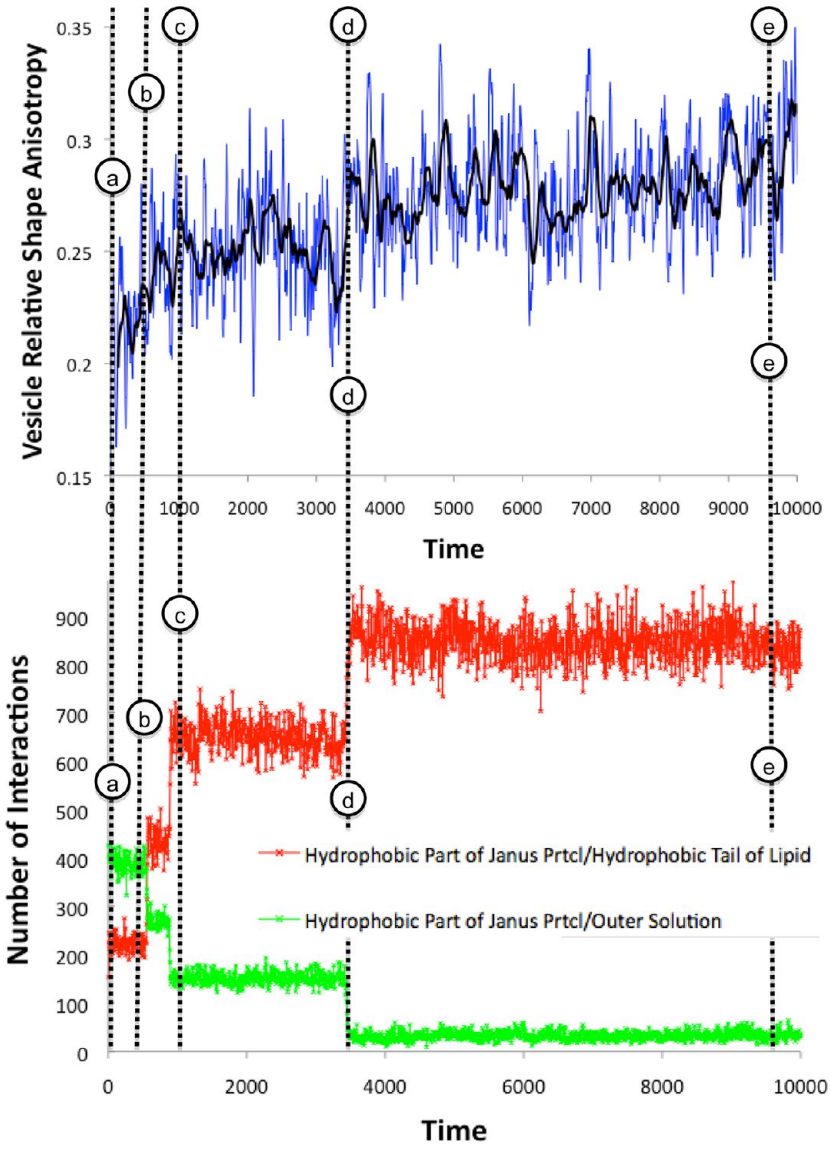

Figure 8. (Top) Relative shape anisotropy of the vesicle with four Janus particles on the plane. (Bottom) Number interactions between hydrophobic beads of Janus particle and lipid tails (in red) and between hydrophobic beads of Janus particle and solvent (in green). The lines represent times (a) 0, (b) 558, (c) 894, (d) 3444, and (e) 9960, corresponding to snapshots in Figure 7.

Dropping Off Janus Particles on Patterned Surfaces. In the above sections, we pinpointed the range of shear rates, substrate adhesion strengths, and fractions of hydrophobic beads on the Janus particle for which the intact vesicle−particle assembly is successfully transported along the surface. To fully exploit the potential of this nanoscopic cargo carrier, it would be useful to achieve a controlled release or drop off of the attached Janus particle. Potential strategies for realizing a controlled drop off involve tuning either the shear rate or the substrate adhesion strength. Our preliminary results show that increasing the shear rate provides a robust drop off only in the case with particles that encompass the lowest fraction of hydrophobic beads, $\phi = 0.010$. In the other cases, the vesicle is easily ruptured at high shear rates, and the particle is dropped off at random positions on the surface. In other words, variations in $\dot{\gamma}$ do not provide a reliable means of achieving controllable particle drop off. Therefore, we turn to the strategy associated with substrate adhesion and introduce patterned surfaces, that is, substrates with relatively "sticky" domains. The idea of introducing heterogeneity on a surface to control the motion of microcapsules has been implemented in a few previous studies.[18−20] Both mechanically (*e.g.*, different stiffness) and chemically (*e.g.*, different adhesion) patterned surfaces were utilized to regulate the motion effectively.

Herein, we introduce a patch on the surface that exhibits a stronger adhesive interaction with the Janus particle than the rest of the surface. This patch is characterized by $K_{patch/Janus} = 12$; notably, the adhesive

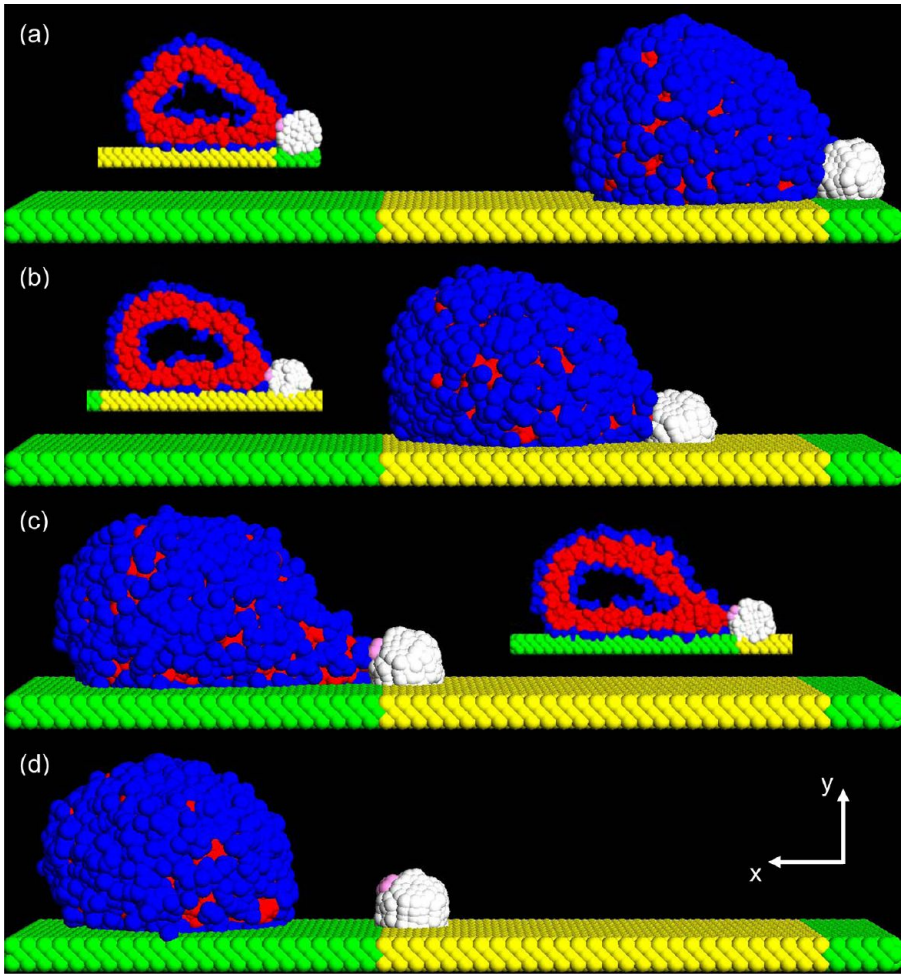

Figure 9. Snapshots of the system in which the vesicle drops off a Janus particle with a fraction of hydrophobic beads $\phi = 0.010$ (a total of 4 hydrophobic beads) on a "sticky" patch (colored in yellow) for shear rate $\dot{\gamma} = 0.015$ and bond constants $K_{sub/lipid} = K_{patch/lipid} = 4$, $K_{sub/Janus} = 8$ and $K_{patch/Janus} = 12$. The snapshots are taken at times (a) 160, (b) 576, (c) 1254, and (d) 1300. The insets in (a–c) are the cross-sectional views of the vesicle–Janus particle assembly.

interaction between the patch and the vesicle is the same as that for the rest of the surface (*i.e.*, $K_{patch/lipid} = K_{sub/lipid} = 4$). The patch is 30.25 units in width and lies perpendicular to the flow direction. These simulations are performed in two stages. We first carry out a separate simulation involving the homogeneous surface described above and allow the vesicle to interact with a Janus particle, setting $K_{sub/Janus} = 8$ and the shear rate $\dot{\gamma} = 0.015$. These simulations yield the morphology of the vesicle–particle assembly. This specific structure is then introduced in front of the patch on the heterogeneous substrate, as shown in Figure 9.

When the fluid-driven vesicle–particle assembly encounters the patch, we observe that the Janus particle with the smallest fraction of hydrophobic beads, $\phi = 0.010$, is arrested at the second patch–substrate interface, as shown in Figure 9c. On the other hand, the vesicle continues to move forward along the substrate (since it does not experience a more adhesive interaction with the patch). Notably, the particle detaches cleanly from the vesicle, without removing lipids from the membrane. The number of hydrophobic particle bead/lipid tail interactions drops to 0 (see Figure S4 in Supporting Information), which confirms the complete detachment. The drop off is robust for four independent runs. Hence, for this set of parameters, the particle can be controllably dropped off at a particular location on the heterogeneous surface.

The patch introduces sharp adhesion gradients at two patch–substrate interfaces, which also correspond to discontinuities in the potential. When the particle meets the first interface, the motion is from the region of weaker surface adhesion to the region of stronger adhesion. The favorable enthalpic force induced by the adhesion gradient facilitates the transport of the particle across the interface since the force points along the direction of motion. The second interface, however, presents a barrier in the potential for the particle's motion, and the net enthalpic force is directed in the direction opposite to the motion and, hence, inhibits the movement of the particle. The interaction between the Janus particle and the potential barrier eventually yields the drop off.

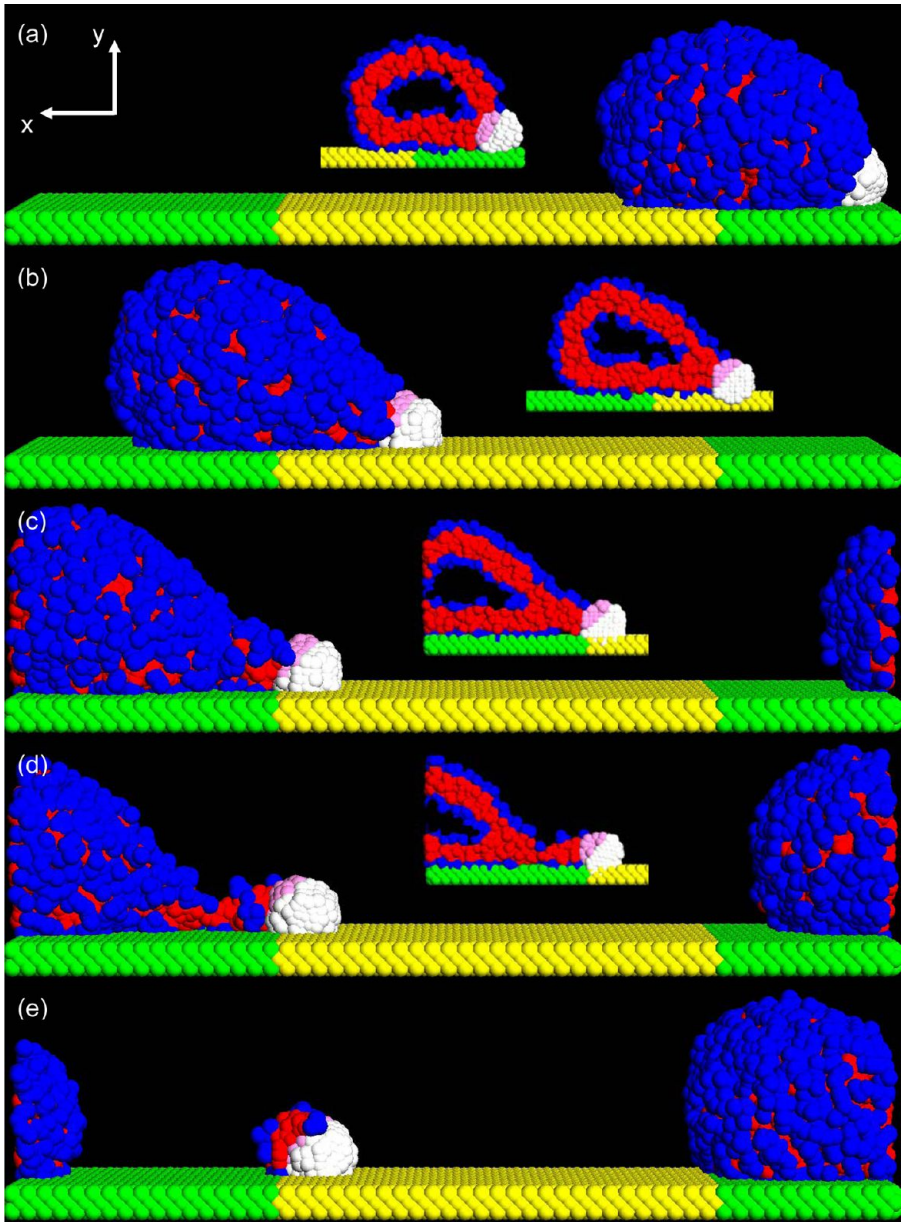

Figure 10. Snapshots of the system in which the vesicle drops off a Janus particle with a fraction of hydrophobic beads $\phi = 0.245$ (a total of 96 hydrophobic beads) on a sticky patch for shear rate $\dot{\gamma} = 0.015$ and bond constants $K_{sub/lipid} = K_{patch/lipid} = 4$, $K_{sub/Janus} = 8$, and $K_{patch/Janus} = 12$. The snapshots are taken at times (a) 308, (b) 1000, (c) 2100, (d) 3092, and (e) 3256. The insets are the cross-sectional views of the vesicle−Janus particle assembly.

The underlying physics of this drop off process also played a role in separating motile capsules as they moved along a heterogeneous surface.[20]

Another drop off scenario is observed for Janus particles with all of the higher fractions of hydrophobic beads considered herein: ϕ = 0.061, 0.140, 0.245, and 0.367. In these cases, some of the lipids become detached from the vesicle as the particle is dropped off, as shown in Figure 10. To characterize this drop off scenario, for a simulation run presented in Figure 10, we measured the number of specific bead−bead interactions as indicated in Figure 11. The drop off process is initiated at time 1220 when the particle is arrested at the second interface. As the vesicle becomes elongated, the number of interactions between the hydrophobic moieties on the lipids and the particle decreases and the hydrophobic portion of the particle becomes exposed to the outer solution (Figure 10c). (Note the significant increase in the number of hydrophobic particle bead/outer solution bead interactions and the corresponding decrease in the number of hydrophobic particle bead/hydrophobic lipid tail interactions from time 1220 to (c).)

With the further stretching of the vesicle, there is an increase in the number of hydrophobic lipid tail/outer solution interactions, indicating that the hydrophobic part of the membrane is exposed to the outer solution. With exposure of the hydrophobic portions of the

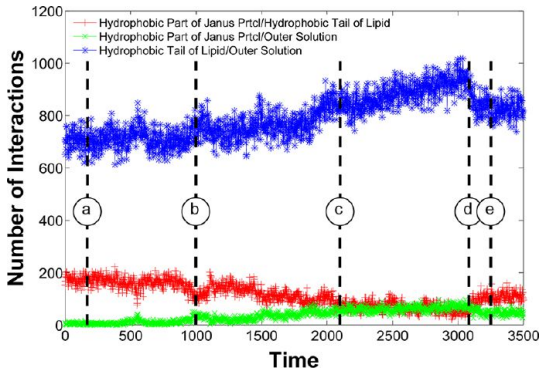

Figure 11. Temporal evolution of the number of interactions between the hydrophobic beads of the Janus particle and the outer solution (green crosses), between the hydrophobic beads of the Janus particle and the hydrophobic beads of the lipids (red pluses), and between the hydrophobic beads of the lipids and the outer solution (blue asterisks), for the simulation shown in Figure 10. The annotations with the letters a–e correspond to the frames Figure 10a–e, respectively.

membrane, breakage between the remaining hydrophobic particle bead/hydrophobic lipid tail interactions is energetically unfavorable. Instead, the stress in the assembly tends to stretch the vesicle and form a neck connecting it with the hydrophobic portion of the Janus particle. Therefore, the number of lipid tail/outer solution interactions continues to rise, while the number of interactions between the hydrophobic particle beads/outer solution and hydrophobic particle beads/hydrophobic lipid tails reaches a constant value (Figure 11, time (c) to (d)). The stress in the vesicle eventually ruptures the neck, and the particle is dropped off with a few residual lipid molecules. The rupture releases the stress, and the vesicle continues to be transported along the substrate, as reflected by a sudden drop in the number of hydrophobic lipid tail/outer solution interactions. Independent runs at each value of ϕ confirm that the latter rupture scenario is robust for the Janus particles with ϕ = 0.061, 0.140, 0.245, and 0.367.

In addition to the value of ϕ, the adhesion strength between the patch and the particle, $K_{patch/Janus}$, plays a vital role in the drop off process. The phase map in Figure S5 indicates how this parameter affects the drop off process for different values of ϕ and $10 \leq K_{patch/Janus} \leq 12$. When $K_{patch/Janus}$ is relatively weak, the potential barrier at the second patch/substrate interface is too shallow to induce the drop off of the particle. The whole assembly passes the yellow patch and keeps moving along the substrate. As $K_{patch/Janus}$ is increased, making the patch more sticky for the particle, the potential barrier can impose sufficiently strong force to arrest the particle and result in particles with low ratios of hydrophobic beads ϕ being successfully dropped off at the second edge of the patch. Particles characterized by higher values of ϕ experience a drag force from the vesicle that is sufficient to overcome the opposing enthalpic force, and the particle passes the patch. As mentioned above, only the particle with the lowest fraction of hydrophobic beads ϕ = 0.010 produces clean detachment; the drop off of particles with higher fractions of ϕ = 0.061, 0.140, 0.245, and 0.367 all involves the rupture of the vesicle.

Finally, our simulations show a relatively minor effect of the imposed shear rates within the range of the shear rates considered herein (see Figure S5). This study indicates that the properties of the patch could be tailored to achieve optimal pick up and delivery. These patches can be utilized in microfluidic devices to sort Janus particles based on their chemical composition.

CONCLUSIONS

To provide effective guidelines for utilizing lipid vesicles as cargo carriers in micro- and nanofluidic devices, we performed computer simulations to probe the interactions between a nanoscopic vesicle and spherical Janus particles in the presence of an imposed flow. The vesicle and Janus nanoparticles were placed on a hydrophilic substrate and immersed in a hydrophilic solution. The favorable enthalpic interactions between the hydrophobic sites on the Janus particle and the hydrophobic interior of the lipid bilayer enabled the fluid-driven vesicle to successfully adsorb or "pick up" the nanoparticle. We systematically varied the chemical composition of the nanoparticles, the adhesion strength between the nanoparticle and substrate, and the shear rate and consequently identified the appropriate range of parameters that leads to robust carrier cargo assembly, with the hydrophobic portion of the particle being localized within the hydrophobic domain of the bilayer. In general, this self-assembly and, hence, optimal pick up is achieved in scenarios involving the following: Janus particles with a large hydrophobic component, low substrate adhesions, and low shear rates. We also examined the payload capacity of the nanoscale vesicle by simulating the interaction between a vesicle and multiple Janus particles and observed that these vesicles can successfully pick up up to four particles.

We then considered scenarios that would lead to controlled drop off the adsorbed particles, so that the vesicles could provide a means of controllably delivering nanoparticles to specified locations within the fluidic chambers. Specifically, we designed a chemically heterogeneous substrate that encompasses a sticky patch, which has a stronger adhesive interaction with the particle than the rest of the substrate. We isolated the range of parameters where the vesicle can drop off the particles and remain intact as it keeps moving along the surface. We also pinpointed the parameters where some lipids that are bound to the particle detach from the bilayer as the particle is deposited, but the vesicle is not completely ruptured.

Overall, our findings provide insight into harnessing fluid-driven vesicles to controllably transport nanoscopic cargo in nano- and microfludic devices. The results suggest that the vesicles could be used to collect and remove debris from the lower surface of these devices. Alternatively, through their ability to deliver and deposit the particles, these vesicles can play an important role in facilitating the bottom-up assembly of particles within these fluid-filled chambers.

METHODOLOGY

DPD method can be viewed as a coarse-grained molecular dynamics (MD) approach. Similar to MD simulations, DPD captures the time evolution of a many-body system through the numerical integration of Newton's equation of motion, $m d\mathbf{v}_i/dt = \mathbf{f}_i$, where the mass m of a bead is set equal to 1. The force acting on a bead consists of three parts, each of which is pairwise additive: $\mathbf{f}_i(t) = \sum(\mathbf{F}_{ij}^{C} + \mathbf{F}_{ij}^{D} + \mathbf{F}_{ij}^{R})$, where the sum runs over all beads j within a certain cutoff radius r_c. We take r_c as our characteristic length scale and set the dimensionless value as $r_c = 1$. The conservative force is a soft, repulsive force given by $\mathbf{F}_{ij}^{C} = a_{ij}(1 - r_{ij})\hat{\mathbf{r}}_{ij}$, where a_{ij} is the maximum repulsion between beads i and j, $\mathbf{r}_{ij} = \mathbf{r}_i - \mathbf{r}_j$, $r_{ij} = |\mathbf{r}_{ij}|$, and $\hat{\mathbf{r}}_{ij} = \mathbf{r}_{ij}/|\mathbf{r}_{ij}|$. The drag force is $\mathbf{F}_{ij}^{D} = -\gamma\omega_D(r_{ij})(\hat{\mathbf{r}}_{ij} \cdot \mathbf{v}_{ij})\hat{\mathbf{r}}_{ij}$, where γ is a simulation parameter related to viscosity, ω_D is a weight function that goes to 0 at r_c, and $\mathbf{v}_{ij} = \mathbf{v}_i - \mathbf{v}_j$. The random force is $\mathbf{F}_{ij}^{R} = \sigma\omega_R(r_{ij})\xi_{ij}\hat{\mathbf{r}}_{ij}$, where ξ_{ij} is a zero-mean Gaussian random variable of unit variance and $\sigma^2 = 2k_BT\gamma$. Finally, we use $\omega_D(r_{ij}) = \omega_R(r_{ij})^2 = (1 - r_{ij})^2$ for $r_{ij} < 1$.[12] Because all three of these forces conserve momentum locally, hydrodynamic behavior emerges even in systems containing only a few hundred particles.[8,11,12] The equations of motion are integrated in time with a modified velocity-Verlet algorithm.[21] As per convention, we take k_BT as the characteristic energy scale in our simulations, with $k_BT = 1$. The characteristic time scale is then defined as $\tau = (mr_c^2/k_BT)^{1/2} = 1$. The remaining simulation parameters are $\sigma = 3$ and $\Delta t = 0.02\tau$, with a total bead number density of $\rho = 3$ and a dimensionless value of $r_c = 1$.[12,22]

The vesicles in our systems are self-assembled from short, twin-tailed lipids; Figure 1a shows a vesicle composed of 586 such lipids. Each amphiphilic lipid is composed of nine beads, with three hydrophilic beads forming the head and six hydrophobic beads contributing to the two tails, as shown in Figure 1b.[3] The bonds between the lipid beads are represented by the harmonic spring potential $E_{bond} = K_{bond}((r - b)/r_c)^2$, where K_{bond} is the bond constant and b is the equilibrium bond length. Here, we set $K_{bond} = 64$ and $b = 0.5$.[22] We also insert a weaker bond ($K_{bond} = 16$) between the first beads (nearest the hydrophilic head) on the two tails to keep the tails oriented in the same direction. Additionally, we include a three-body stiffness potential along the lipids' tails of the form $E_{angle} = K_{angle}(1 + \cos\theta)$, where θ is the angle formed by three adjacent beads,[22,23] and we set the coefficient to $K_{angle} = 5$. This stiffness term increases the stability and bending rigidity of the bilayers.[22]

Each Janus nanoparticle is formed from 392 beads, which are arranged in a face-centered cubic (fcc) lattice structure, with a cube side length of 0.7. The permanent harmonic spring-like bonds between the beads in the nanoparticle are characterized by $K_{bond} = 64$ and two equilibrium lengths $b = 0.7$ and $b = 0.7/\sqrt{2}$ (set according to the spacing between the beads in the fcc lattice). In our reference case, the nanoparticle is divided symmetrically into hydrophobic and hydrophilic parts (see Figure 1c). The fraction of hydrophobic beads in the Janus particle, ϕ, is defined as the number of hydrophobic beads divided by the total 392 beads. In addition to symmetric particles with $\phi = 0.5$, we simulate asymmetric Janus particles by varying ϕ. We vary ϕ by replacing (layer-by-layer) hydrophobic beads with the same number of hydrophilic beads. The asymmetric particles investigated here have $\phi = 0.367$, 0.245, 0.140, 0.061, and 0.010.

The substrate is made up of 5940 frozen hydrophilic beads arranged in a fcc lattice structure of a number density $\rho \approx 3$. We assume that the substrate is adhesive to the nanoscopic vesicle. To model the adhesive nature of the surface, each hydrophilic bead in the vesicle that is in contact with the surface can form a bond with this substrate. The bond between a hydrophilic bead and a substrate bead is modeled by a truncated Hookean spring potential $F_{sub/lipid} = -K_{sub/lipid}(r_{ij} - b)$, which is widely used in other mesoscopic simulations.[24,25] Here, b corresponds to the equilibrium bond length (set at $b = 0.5$) and $K_{sub/lipid}$ is the effective strength of the interaction. These bonds can break when their length exceeds a critical value (*i.e.*, $r_{ij} > r_c$). Furthermore, new bonds can form when the distance between a hydrophilic bead in the vesicle is less than a critical distance from the surface site (*i.e.*, $r_{ij} < r_c$).

In the presence of an applied shear, some fraction of these bonds will break. Importantly, however, the imposed flow also brings the vesicles in contact with new sites further along the surface, and hence, these components can form new bonds with the substrate. Given the number of beads that lie within a distance of $r_{ij} < r_c$ from the surface, the net effect of these bonding interactions is to create an adhesive force that prevents the vesicle from detaching from the substrate but nonetheless allows the fluid-driven vesicle to slide along the substrate.

We specified the strength of the adhesion by setting $K_{sub/lipid} = 4$, which yields an adhesion energy per unit area of $\approx 10^{-2}$ J/m^2 between the nanoscale vesicle and the substrate. The adhesion energy is on the same scale as used in other coarse-grained MD simulations for supported lipid bilayers,[26,27] as well as MD simulations with fully atomistic representations.[28] Notably, this value is also on the same scale as experimental values for the adhesion energy of ligand−receptor bonds.[29] We also apply the adhesion between the Janus particles and the substrate in the similar manner with $6 \leq K_{sub/Janus} \leq 12$, which represents a stronger adhesion.

Hydrophilic solution beads fill the interior of the vesicle and the remaining volume of the periodic simulation box. Unless stated otherwise, the size of the box is $60.5 \times 40.0 \times 19.8$ (we choose the dimensions of the box in x- and z-directions to match the lattice constant of the substrate). The nature of the hydrophilic/hydrophobic interactions between the beads is captured by specifying the repulsive interactions between the components. Our choices for the interaction parameters between the components, a_{ij}, are as follows:[3] for any two beads of the same type, we set the repulsion parameter to be $a_{ij} = 25$ (measured in units of k_BT/r_c), and the value of the interaction parameter between the hydrophobic−hydrophilic moieties is specified by $a_{ij} = 100$. These values were used in a number of previous DPD simulations of lipid bilayers,[22,30] and as previously observed,[22,23] we find that lipids spontaneously self-assemble into bilayers[15] or vesicles for these interaction parameters.[3,31]

As noted in the introduction, our vesicles and Janus nanoparticles are driven to move along the substrate by an imposed shear flow. We set the substrate in the $x-z$ plane (at $y = 0$) and apply shear to the system in the y-direction. The shear flow is imposed by the Lees−Edwards periodic boundary conditions by displacing the images of the periodic simulation box at two boundaries, $y = 10$ and $y = -10$.[32] The resulting shear flow has a velocity in the x-direction of a magnitude given by $V_{sh} = \dot{\gamma}y$, where $\dot{\gamma}$ is the shear rate. Below, we focus on shear rates within the range $0.015 \leq \dot{\gamma} \leq 0.035$. It is worth noting that higher shear rates cause the rupture of the vesicle.

The above simulation parameters can be related to physical length and time scales by examining the properties of a tensionless membrane.[22] The lipids in our investigations represent DPPC (dipalmitoylphosphatidycholine, $C_{40}H_{80}NO_8P$). Typical experimental measurements of DPPC membranes[22] in a tensionless state yield an equilibrium area per lipid of

approximately 0.6 nm^2. This value can be used to establish a dimensional length scale in the DPD simulations and gives r_c = 0.67 nm.[22] The DPD time scale τ can be estimated from the in-plane diffusion constant of lipids, which, for a flat DPPC membrane, has been measured[22] as $D = 5\ \mu m^2/s$. By matching the latter value to the diffusion constant in the simulation, one can obtain τ = 7.2 ns and, for a single time step, $\Delta t = 0.02\tau$ = 0.14 ns.[22] Hence, the radius of the Janus particle and the outer radius of the lipid vesicle[17] can be estimated as ~1.4 and ~5.0 nm, respectively. The range of the shear rates in our system corresponds to 2.08×10^6 to $4.86 \times 10^6\ s^{-1}$; these shear rates are of the same order of magnitude as those used in high shear rate experiments in microfluidic devices.[33] The resulting velocity of a particle moving along the substrate is on the order of 5 mm/s, which is within the range of operating velocities in a variety of microfluidic devices.[34] (The latter value corresponds to the dimensionless velocity 0.05 in the simulations.) At these velocities, the corresponding Peclet number can be estimated roughly as Pe ~ 100,[35] and hence, the motion of the vesicle is dominated by advection.

The above correlations between the simulation parameters and physical values provide useful guidelines for experimentally realizing the system described above. In particular, the substrate could be functionalized with ligands (including proteins[37] and peptides[38]) that have an affinity to the surface of the vesicles that is characteristic of the ligand−receptor interactions noted above[29] and, thus, could localize the vesicles on the substrate[37,38] until the imposed shear would dislodge them. The ligands on the substrate could also have an affinity for the hydrophilic surface of the Janus particle. Namely, researchers have developed a range of methods that utilize a variety of ligands to produce Janus nanoparticles with specified hydrophobic and hydrophilic areas.[39] Through the appropriate choice of hydrophilic moieties on the Janus particles, the functionalized surface could exhibit an affinity to the hydrophilic regions of these particles, as well as the hydrophilic surface of the vesicles. A variety of microcontact printing techniques[40] can be used to make the patterned surfaces needed for the particle drop off studies. In particular, *via* the latter method, the desired ligands, which have a stronger binding to the hydrophilic portion of the Janus particles than the rest of the surface, can be printed at a specified region of the surface. In summary, with the possible functionalization of the vesicles,[37] Janus particles,[39] and substrate,[37,38,40] researchers have a wide parameter space to choose from in tailoring the system to match the physical values that correspond to the simulation parameters.

Conflict of Interest: The authors declare no competing financial interest.

Acknowledgment. A.C.B. gratefully acknowledges funding from the National Science Foundation for partial support of I.S. and X.Y., the Army Research Office for partial support of E.J.C. and N.M.M., and the Department of Energy for partial support of G.T.M. and O.K.

Supporting Information Available: A figure showing snapshots of the system with a Janus particle that encompasses a total of four hydrophobic beads (fraction of hydrophobic beads $\phi = 0.010$). Phase map for a lipid vesicle picking up single Janus particle. Plot that shows the temporal evolution of the number of interactions in a system involving four Janus particles. Plot for the temporal evolution of the number of interactions in the simulations involving a surface patch. Phase map for a lipid vesicle dropping of single Janus particle on a "sticky" patch. This material is available free of charge *via* the Internet at http://pubs.acs.org.

REFERENCES AND NOTES

1. Jahn, A.; Stavis, S. M.; Hong, J. S.; Vreeland, W. N.; DeVoe, D. L.; Gaitan, M. Microfluidic Mixing and the Formation of Nanoscale Lipid Vesicles. *ACS Nano* **2010**, *4*, 2077–2087.
2. Yang, K.; Ma, Y. Q. Computer Simulation of the Translocation of Nanoparticles with Different Shapes across a Lipid Bilayer. *Nat. Nanotechnol.* **2010**, *5*, 579–583.
3. Dutt, M.; Nayhouse, M. J.; Kuksenok, O.; Little, S. R.; Balazs, A. C. Interactions of End-Functionalized Nanotubes with Lipid Vesicles: Spontaneous Insertion and Nanotube Self-Organization. *Curr. Nanosci.* **2011**, *7*, 699–715.
4. Vácha, R.; Martinez-Veracoechea, F. J.; Frenkel, D. Receptor-Mediated Endocytosis of Nanoparticles of Various Shapes. *Nano Lett.* **2011**, *11*, 5391–5395.
5. Van Lehn, R. C.; Alexander-Katz, A. Penetration of Lipid Bilayers by Nanoparticles with Environmentally-Responsive Surfaces: Simulations and Theory. *Soft Matter* **2011**, *7*, 11392–11404.
6. Yue, T.; Zhang, X. Molecular Understanding of Receptor-Mediated Membrane Responses to Ligand-Coated Nanoparticles. *Soft Matter* **2011**, *7*, 9104–9112.
7. Christensen, S. M.; Bolinger, P. Y.; Hatzakis, N. S.; Mortensen, M. W.; Stamou, D. Mixing Subattolitre Volumes in a Quantitative and Highly Parallel Manner with Soft Matter Nanofluidics. *Nat. Nanotechnol.* **2012**, *7*, 51–55.
8. Hoogerbrugge, P. J.; Koelman, J. M. V. A. Simulating Microscopic Hydrodynamic Phenomena with Dissipative Particle Dynamics. *Europhys. Lett.* **1992**, *19*, 155–160.
9. Koelman, J. M. V. A.; Hoogerbrugge, P. J. Dynamic Simulations of Hard-Sphere Suspensions under Steady Shear. *Europhys. Lett.* **1993**, *21*, 363–368.
10. Español, P.; Warren, P. Statistical Mechanics of Dissipative Particle Dynamics. *Europhys. Lett.* **1995**, *30*, 191–196.
11. Español, P. Hydrodynamics from Dissipative Particle Dynamics. *Phys. Rev. E* **1995**, *52*, 1734–1742.
12. Groot, R. D.; Warren, P. B. Dissipative Particle Dynamics: Bridging the Gap between Atomistic and Mesoscopic Simulation. *J. Chem. Phys.* **1997**, *107*, 4423–4435.
13. Pivkin, I. V.; Karniadakis, G. E. A New Method To Impose No-Slip Boundary Conditions in Dissipative Particle Dynamics. *J. Comput. Phys.* **2005**, *207*, 114–128.
14. Warren, P. B. Vapor−Liquid Coexistence in Many-Body Dissipative Particle Dynamics. *Phys. Rev. E* **2003**, *68*, 066702.
15. Dutt, M.; Kuksenok, O.; Little, S. R.; Balazs, A. C. Forming Transmembrane Channels Using End-Functionalized Nanotubes. *Nanoscale* **2011**, *3*, 240–250.
16. Noguchi, H.; Gompper, G. Dynamics of Vesicle Self-Assembly and Dissolution. *J. Chem. Phys.* **2006**, *125*, 164908.
17. The outer (inner) radius of the vesicle is measured as the average distance between the outer (inner) lipid head beads and the center of mass of the vesicle. The outer radius is 7.50, and the inner radius is 3.91. The size of the Janus particle is 2.11.
18. Alexeev, A.; Verberg, R.; Balazs, A. C. Patterned Surfaces Segregate Compliant Microcapsules. *Langmuir* **2007**, *23*, 983–987.
19. Usta, O. B.; Alexeev, A.; Balazs, A. C. Fork in the Road: Patterned Surfaces Direct Microcapsules To Make a Decision. *Langmuir* **2007**, *23*, 10887–10890.
20. Kolmakov, G. V.; Yashin, V. V.; Levitan, S. P.; Balazs, A. C. Designing Self-Propelled Microcapsules for Pick-up and Delivery of Microscopic Cargo. *Soft Matter* **2011**, *7*, 3168–3176.
21. Plimpton, S. Fast Parallel Algorithms for Short-Range Molecular Dynamics. *J. Comput. Phys.* **1995**, *117*, 1–19.
22. Smith, K. A.; Jasnow, D.; Balazs, A. C. Designing Synthetic Vesicles that Engulf Nanoscopic Particles. *J. Chem. Phys.* **2007**, *127*, 084703.
23. Shillcock, J. C.; Lipowsky, R. Equilibrium Structure and Lateral Stress Distribution of Amphiphilic Bilayers from Dissipative Particle Dynamics Simulations. *J. Chem. Phys.* **2002**, *117*, 5048–5061.
24. Maresov, E. A.; Kolmakov, G. V.; Yashin, V. V.; Van Vliet, K. J.; Balazs, A. C. Modeling the Making and Breaking of Bonds as an Elastic Microcapsule Moves over a Compliant Substrate. *Soft Matter* **2012**, *8*, 77–85.
25. Roiter, Y.; Ornatska, M.; Rammohan, A. R.; Balakrishnan, J.; Heine, D. R.; Minko, S. Interaction of Lipid Membrane with Nanostructured Surfaces. *Langmuir* **2009**, *25*, 6287–6299.
26. Hoopes, M. I.; Longo, M. L.; Faller, R. Computational Modeling of Curvature Effects in Supported Lipid Bilayers. *Curr. Nanosci.* **2011**, *7*, 716–720.

27. Hoopes, M. I.; Deserno, M.; Longo, M. L.; Faller, R. Coarse-Grained Modeling of Interactions of Lipid Bilayers with Supports. *J. Chem. Phys.* **2008**, *129*, 175102.
28. Heine, D. R.; Rammohan, A. R.; Balakrishnan, J. Atomistic Simulations of the Interaction between Lipid Bilayers and Substrates. *Mol. Simulat.* **2007**, *33*, 391–397.
29. Israelachvili, J. N. *Intermolecular and Surface Forces*, 3rd ed.; Elsevier: Amsterdam, 2011.
30. Alexeev, A.; Upsal, W. E.; Balazs, A. C. Harnessing Janus Nanoparticles To Create Controllable Pores in Membranes. *ACS Nano* **2008**, *2*, 1117–1122.
31. Dutt, M.; Kuksenok, O.; Nayhouse, M. J.; Little, S. R.; Balazs, A. C. Modeling the Self-Assembly of Lipids and Nanotubes in Solution: Forming Vesicles and Bicelles with Transmembrane Nanotube Channels. *ACS Nano* **2011**, *5*, 4769–4782.
32. Lees, A. W.; Edwards, S. F. Computer Study of Transport Processes under Extreme Conditions. *J. Phys. C* **1972**, *5*, 1921.
33. Pipe, C. J.; McKinley, G. H. Microfluidic Rheometry. *Mech. Res. Commun.* **2009**, *36*, 110–120.
34. Squires, T. M.; Quake, S. R. Microfluidics: Fluid Physics at the Nanoliter Scale. *Rev. Mod. Phys.* **2005**, *77*, 977–1026.
35. To estimate the Peclet number in our system, we approximated the in-plane diffusion coefficient of the vesicle as $D_v = 0.2\ \mu m^2/s$, which corresponds to the experimentally measured value for the diffusion coefficient of a vesicle tethered to a lipid bilayer.[36] While the sizes of the tethered vesicles in the latter study (ranging between 30 and 200 nm) were somewhat larger than in our case, the authors showed that value of the lateral diffusion coefficient was insensitive to the vesicle size. Hence, we can estimate the Peclet number in our system as $Pe = LU/D_v \sim 10^2$, where as a characteristic length scale we take the radius of the vesicle, $L \sim 5$ nm and $U \sim 5$ mm/s (see Methodology).
36. Yoshina-Isii, C.; Chan, Y.-H. M.; Johnson, J. M.; Jung, Li. A.; Lenz, P.; Boxer, S. G. Diffusion Dynamics of Vesicles Tethered to a Fluid Supported Bilayer by Single-Particle Tracking. *Langmuir* **2006**, *22*, 5682–5689.
37. Jung, L. S.; Shumaker-Parry, J. S.; Campbell, C. T.; Yee, S. S.; Gelb, M. H. Quantification of Tight Binding to Surface-Immobilized Phospholipid Vesicles Using Surface Plasmon Resonance: Binding Constant of Phospholipase A_2. *J. Am. Chem. Soc.* **2000**, *122*, 4177–4184.
38. Voskuhl, J.; Wendeln, C.; Versluis, F.; Fritz, E.-C.; Roling, O.; Zope, H.; Schulz, C.; Rinnen, S.; Arlinghaus, H. F.; Ravoo, B. J.; Kros, A. Immobilization of Liposomes and Vesicles on Patterned Surfaces by a Peptide Coiled-Coil Binding Motif. *Angew. Chem., Int. Ed.* **2012**, *51*, 12616–12620.
39. Lattuada, M.; Hatton, T. A. Synthesis, Properties and Applications of Janus Nanoparticles. *Nano Today* **2011**, *6*, 286–308.
40. Ruiz, S. A.; Chen, C. S. Microcontact Printing: A Tool To Pattern. *Soft Matter* **2007**, *3*, 168–177.